# Software defined radio based frequency modulated continuous wave ground penetrating radar

Patrick Fiske<sup>a</sup>, Dryver Huston<sup>\*b</sup>, Tian Xia<sup>a</sup>

<sup>a</sup> Electrical and Biomedical Engineering Dept., Univ. of Vermont, 33 Colchester Ave., Burlington, VT, USA 05405; <sup>b</sup>Mechanical Engineering Dept., Univ. of Vermont, 33 Colchester Ave., Burlington, VT, USA 05405

## **ABSTRACT**

Frequency modulated continuous wave (FMCW) radar allows for a wide range of research applications. One primary use of this technology which is explored in this paper is the ground penetrating radar. To achieve high sensing performance, wide-band spectral reconstruction and sophisticated image reconstruction algorithm have been developed to overcome hardware limitations. Applications and future work include Synthetic Aperture Radar (SAR) imaging, innovative GPR, and unmanned aerial vehicle (UAV) radar systems.

**Keywords:** Ground penetrating radar, frequency modulated continuous wave, chirp, software-defined radar

## 1. INTRODUCTION

In more recent times, the use of ground penetrating radars has increased in academia and in civil applications [1-3]. The resulting improvements have allowed for more affordable systems creating a cycle of compounding innovations. A current system is in place but is limited by the techniques and implementation. This project overcomes such limitations and has several benefits that will expand the use of the system. With the proposed method, several techniques to design GPR will be viable, along with Synthetic Aperture Radar (SAR) applications. Not all of these will be explored in depth for, but the development of the GPR system with these capabilities will be conducted. Through the use of Software Defined Radio, (SDR), the system will be fully modular within the limitations of the equipment specifications. As a GPR, the system will be capable of detecting subsurface objects along with general target ranging. Through the proposed method, airborne techniques will be possible and currently are undergoing separate development. An airborne system has the potential of landscape SAR imaging for ground penetrating applications [4], providing endless possibilities for expansion and innovation [5-9]. The development of this radar system can be broken down into a few main sections, hardware, hardware corrections, and software. Topics discussed will begin with a brief overview of the hardware, signal generation and results.

## 2. SIGNAL GENERATION

## 2.1 Wideband Signal for GPR

Signal generation for GPR can be completed with various methods and can be designed for numerous applications. This project focused on developing a wideband chirp to be used in subsurface object detection. The key aspects of this design include a high-resolution radar that can collect data for subsurface image reconstruction in the form of A scans and B scans. The instantaneous bandwidth of the Ettus B210 board will be leveraged to produce multiple sub-pulses at various center frequencies. These sub-pulses will then be frequency shifted and phase corrected to construct a wideband chirp waveform. Various methods will be implemented to correct for hardware deficiencies and signal enhancement.

<sup>\*</sup>dryver.huston@uvm.edu; phone 1 802 656-1922

## 2.2 Designing the sub-pulse

The theoretical waveform that would produce the best results would be a perfectly continuous wideband waveform. Since this is not possible from the instantaneous bandwidth limitations, multiple sub-pulses must be designed and reconstructed to emulate this ideal wideband waveform. For this design, a wideband signal of 4GHz will be reconstructed with various sub-pulses of 16MHz each. A best-case design would have been to use 56MHz sub-pulses, but due to hardware limitations 16MHz was chosen to be the maximum obtainable bandwidth. Each sub-pulse was chosen to be a chirp signal for its many advantages over impulse radar and is mathematically represented as,

$$W[t_m] = A[t_m]e^{j\pi Kt^*t}$$
 (1)

Where K is the chirp rate defined as the sub-pulse bandwidth divided by the period. This equation was used to model and simulate the chirp signal with a matched filter implementation.

#### 2.3 Pulse Compression and Stepped Frequency

Pulse compression, otherwise known as matched filtering, was used to calculate the phase shift between the sent and received chirp. With one sub-pulse, the chirp would be able to detect an object by compressing the signal to achieve the frequency domain response in equation (2), where n is the  $n^{th}$  sub-pulse and  $f_k$  is the frequency index.

$$D_n[f_k] = Z_n[f_k] * V_n[f_k]$$
(2)

To reconstruct multiple sub-pulses the stepped frequency method was used. Each pulse was fully transmitted and received before stepping to the next center frequency. Figure 1 shows a pictorial representation of frequency stacking where each rectangle is a sub-pulse. For implementation, each sub-pulse slightly overlaps others with a two percent random shift for reducing side lobes.

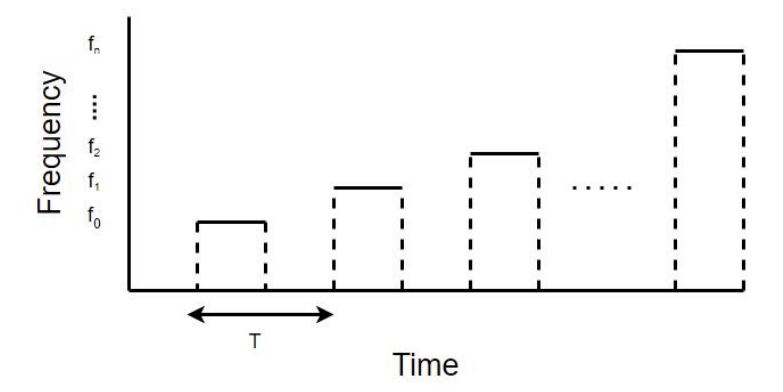


Figure 1, pictorial representation of the frequency stacking method, frequency vs time

# 2.4 Frequency Stacking

As the radar instantaneous bandwidth is limited to values much less than 5GHz, a reconstruction process is required to achieve high bandwidths. The method implemented will be referred to as frequency stacking and can be represented in both the frequency and time domains but is easier to execute in the frequency domain since convolution can be avoided.

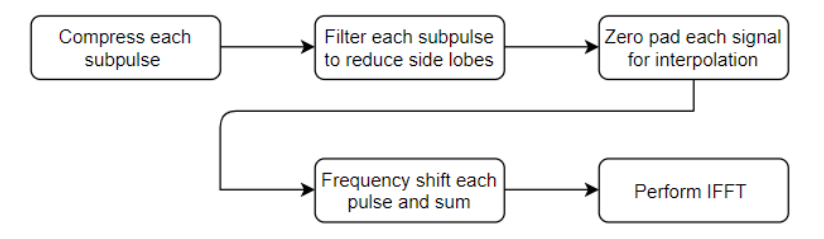


Figure 2, The frequency stacking method

Given the mathematical representations of the signals in each step, a frequency stacking algorithm [10-13] can be leveraged to generate the reconstructed signal. This is the synthetic wideband waveform that when used can create the radar range profile. This method is represented in Figure 2 where first each individual sub-pulse is compressed, filtered, and interpolated. The last steps are to perform frequency and phase corrections and then take the IFFT of the reconstructed wideband waveform. The mathematical representation of the frequency stacking method is shown below.

1: For each sub-pulse signal, take the discrete Fourier Transform to compute the compressed signal.

$$D_{n}[f_{k}] = Z_{n}[f_{k}] * V_{n}[f_{k}]$$
(2)

- 2: Filter each sub-pulse with a desired window function. The bandwidth of this filter should be equivalent to the frequency spacing of the sub-pulses.
- 3: Zero pad each sub-pulse at both ends. To sufficiently up sample the signal pad the front with  $L_{up} = N*L$  where

$$L = f_s * Lo (3)$$

- 4: Perform a circular shift in the frequency domain by  $\Delta f_n$ .
- 5: Sum each of the compressed sub-pulses to obtain the frequency domain response.

$$\mathbf{D}[\mathbf{f}_k] = \sum_{n=0}^{N-1} D_n [f_k - \Delta f_n] rect \left[ \frac{f_k - \Delta f_n}{B_z} \right]$$
 (4)

6: Perform the inverse Fourier Transform to obtain full wideband response

$$d[tm] = d[t_m] = \frac{1}{L_{up}} \sum_{k=0}^{L_{up}-1} D_n[f_k] e^{j2\pi km/L_{up}}$$
(5)

The above algorithm was used to properly reconstruct the synthetic wideband signal. The first step gives the match filter output of each sub-pulse. This is the magnitude and phase response that will need to be combined with the other pulses. Filtering these will ensure there is less noise on the system so when the responses are stacked next to each other there is less additive noise. Circular shifting in step 4 moves the sub-pulse to its appropriate center frequency. This shift is in increments of the center frequency steps to ensure each pulse stacks next to each other. These sub-pulses are then added together to make the wideband waveform described in step 5. Taking the IFFT will calculate the range response forming an A-scan. This A-scan is capable of detecting the reflection imposed by an object with a resolution given by the following equation,

$$\Delta r = \frac{C}{2B} \tag{6}$$

Stacking the A-scans adjacent to each other produces a radargram, also known as a B-scan. The resulting B-scan from testing is seen in figure 6and is colored to emphasize the scan profile.

For this project, each sub-pulse was passed through a Turkey window in MATLAB based on its suppression of distance lobes. Given that the sent pulses each have a bandwidth of 16 MHz, the width of the filter covers only these frequencies. The zero padding was performed on each sub-pulse while being stored into a pre-allocated array. The front end of the pulses was provided L zeros, while the remaining pulses were provided enough zeros to allocate room for the remaining pulses in the same DFT. In the frequency domain, the concatenation of zeros before and after the signal effectively performs sinc interpolation in the time domain. Generally, this up sampling is by a factor of N [7]. Although this introduces a slight error in the reconstructed signal, this has been deemed insignificant in terms of signal resolution[14-17]. The remaining portion of the algorithm was performed exactly as stated and the inverse Fourier transform operated on the reconstructed signal. This process was simulated in full to ensure proper functionality and applied to the final results as seen in later sections.

## 2.5 Phase Correction

By default, the transmit and receive signals do not have coherent phase, and therefore cannot be used without correction. There were two methods used to solve this issue, one being a loopback cable, and the other being a software correction. Since there is a varying phase offset between each sub-pulse of the transmit and receive, convolving the receive signal with a loopback signal solves for the phase error as shown below. The error is represented as the difference between transmit and receive error.

$$\varphi_{e,n} = \varphi t, n - \varphi r, n \tag{7}$$

The loopback allows for a simple calculation of the phase from the collected signal. For this method to work, the transmitter and receiver must be coherent on the software end which was accomplished with the python API provided by Ettus.

#### 2.6 Magnitude Corrections

While performing loopback tests, the results appeared to be accurate within the designed resolution, but when observing the stacked spectrum, it appeared that the signal strength was varying by upwards of 100dB throughout the frequency range. At the time, it was believed that this was a hardware problem and maybe an issue with the transfer function of the splitter or other hardware in use. After a significant amount of troubleshooting, it was realized that the channels also had different gain levels when all parameters were matching. Channel B was about 20dB weaker than Channel A. During loopback matching attenuators were used to help troubleshoot this and the device appeared to be working better. The magnitude of the received time domain signals seemed to hover around values of 0.5mV to 0.9mV and decreased as the

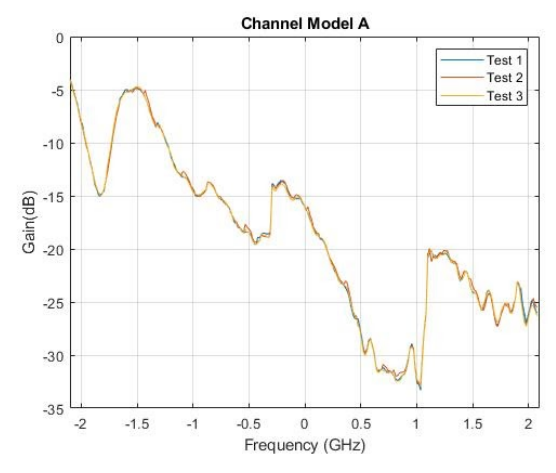


Figure 3, Channel model A of the Ettus B210

frequency increased. When plotting the spectrum, it was obvious that the magnitude was unstable, and without saturating the signal it was difficult and tedious to correct the gains. The overall wideband frequency range was separated into ten sections that all had various gains attempting to correct the problem. Once implemented, the results seem to remain the same as they were before, but now the spectrum was only dropping by 30 to 50 dB.

To solve this persisting issue, a look-up table was generated since sectioning the gains was not sufficient. The idea was to create a table that the python code would reference at each center frequency. The values inside this table would be the correct gain to provide a magnitude normalized to the same value. Through experimental testing it was concluded that the transfer function of the hardware was deterministic, so the look-up table could be generated based on loopback data. Because of this, the first step in constructing this table was to perform a loopback test with the radar and then calculate the gain required.

Figure 3 shows the drop in gain over the entire frequency range of 800MHz-5GHz centered about zero. After some time using the radar, the gain changes appeared to happen at the same frequencies. To quantify the changes and prove that the transfer function was in fact deterministic, figure 3 was produced for multiple trials. Three are shown in the figure, but after a significant amount of use it is safe to say the transfer function can be corrected with a gain table. As previously

noted, the two channels received signals at different strengths, so the process was repeated for the second channel. The results from performing the same procedure on the second channel can be seen in figure 4.

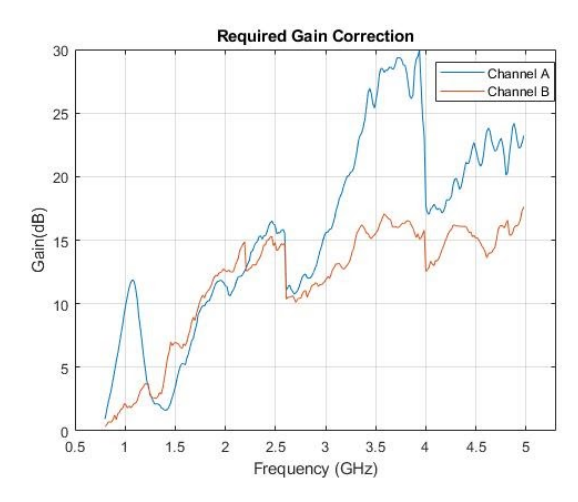


Figure 4, Required gained corrections for both channels of the B210

Comparing the two channel models illustrates that the channels are not off by a set value and a gain table is required for each channel. These values were stored in a matrix, one column for channel A and the other for channel B. The function to assign receive gains was implemented at each frequency step calling this look-up table and pulling the correct value. Plotting the necessary gains to correct the magnitude can be seen in figure 4.

Prior to implementation of the gain control, the A scan produced by the uncorrected data still measures the length of the cable correctly but will not have the designed resolution. Additionally, if the gain was not high enough on the radar, the receive buffer would detect only zeros and the general operation of the device is not always consistent. Pulling the values required from figure 4 and including them in the code as a look-up table produces a consistently working system. The corrected channel model is applied to each test and can be seen in the results.

Using these values allows for the reconstruction process to leverage the full effective bandwidth. The correction of this transfer function actually introduces more side lobes which is expected. Before the low power sub-pulses did not contribute to the resolution, so now every single pulse is considered and the radar achieves the designed effective bandwidth. The additional contribution is also the explanation for the side lobes since they originate from the spectral discontinuities. Additional side lobe suppression was implemented with a grating lobe suppression (GLS)[3] filter. The inversion filter is seen in equation 8, and using it reduces all of the additional side lobes to an insignificant level and is applied to all of the results. M[f] represents and ideal chirp while W[f] is the channel model obtained by the loopback configuration. The equation produces an inverted channel model that will negate the discrepancies introduced from frequency stacking.

$$H(f) = \frac{M[f]}{W[f]} rect\left[\frac{f}{BW}\right], \ W[f] \neq 0$$
(8)

The combination of phase and magnitude corrections paired with frequency stacking allows for the successful implementation of a stepped frequency wideband waveform used for GPR.

## 3. RESULTS

#### 3.1 Results

Before collecting results, the above methods were simulated and fully tested. Simulations were conducted in MATLAB along with most of the post processing. Theoretical waveforms were generated as transmit signals and compared to a delayed version with additional noise. Then the testing began as seen in Figure 6 where a stack of soda cans were taped to a wall. This setup is less than ideal, but due to the COVID-19 restrictions at the time of testing, everything was done without proper lab access.

The wideband reconstruction is shown below, where a 4GHz signal was created. In Figure 5 (left), discontinuities are present where the pulses overlap and the pulses combine both in a constructive and deconstructive manner. Applying the GLS filter removes these overlaps and Figure 5 (right) is produced. Performing the inverse FFT on the corrected SWW gives the range profile for the scan. The GLS filter removed almost all of the grating sidelobes that were impacting the results. Loopback operation was verified before testing with the antennas.

Testing the system with antennas was conducted in the same manner as the loopback configuration. Although the same

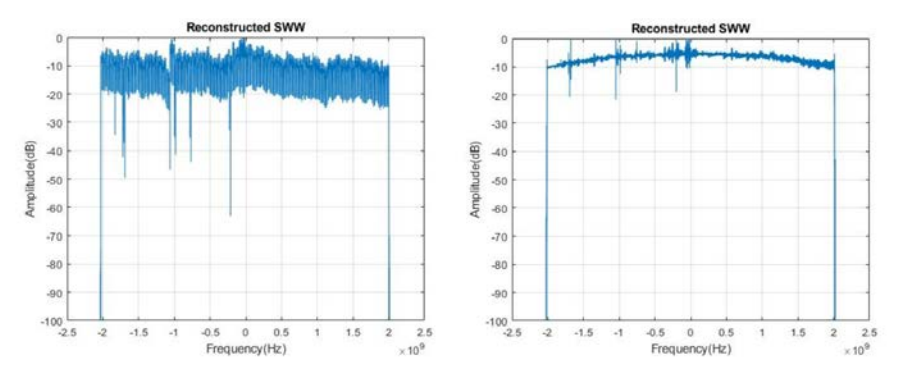


Figure 5, Reconstructed SWW without GLS (left) and Reconstructed SWW with GLS (right)

procedure was used, gain tables specific to the antennas were calculated and applied to the device. Indoor testing was conducted on a stack of soda cans as seen in figure 6. These provided enough of a reflection to create a proper B scan

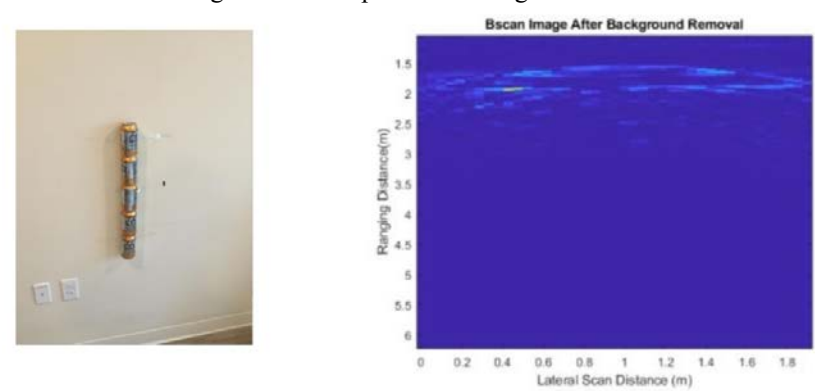


Figure 6, Stacked cans for testing (left) and B-scan results (right)

seen in figure 6, The original B-scan image was enhanced using background removal and smoothing algorithms. The cans were stationed 1.5 meters away from the radar and this correct value is shown in the figure. There is a slight reflection from the wall the cans are taped to, and a stronger reflection from a solid background behind. The lateral scan spanned two meters and consisted of 50 scans.

Without the magnitude correction of the data, this result would not be possible. Even for the loopback configuration the magnitude response dropped significantly. Since there was little noise in the system, the result was extremely accurate. When introducing antennas and noise from the environment, it was nearly impossible to read the results. These corrections proved to be essential in the design of this GPR.

## 4. CONCLUSIONS

In this paper, a software defined ground penetrating radar (GPR) is developed. The study investigates the frequency stacking method to overcome the bandwidth limitation of the hardware. Calibration and filtering algorithms are developed to leverage GPR waveform quality and fidelity.

#### ACKNOWLEDGEMENTS

This material is based upon work supported by the Broad Agency Announcement Program and Cold Regions Research and Engineering Laboratory (ERDC-CRREL) under Contract No. W913E521C0003. Any opinions, findings and conclusion or recommendations expressed in this material are those of the authors and do not necessarily reflect the views of the ERDC-CRREL. This work is also support in part by National Science Foundation (NSF) grants 1647095 and 1640687, and University of Vermont SPARK Fund.

#### REFERENCES

- [1] Huston, D., Xia, T., Zhang, Y., Fan, T., Orfeo, D. and Razinger, J., "Urban underground infrastructure mapping and assessment." In Sensors and Smart Structures Technologies for Civil, Mechanical, and Aerospace Systems 2017 (Vol. 10168, p. 101680M). International Society for Optics and Photonics.Davis, A. R., Bush, C., Harvey, J. C. and Foley, M. F., "Fresnel lenses in rear projection displays," SID Int. Symp. Digest Tech. Papers 32(1), 934-937 (2001).
- [2] Zhang Y, Venkatachalam AS, Xia T. "Ground-penetrating radar railroad ballast inspection with an unsupervised algorithm to boost the region of interest detection efficiency." Journal of Applied Remote Sensing. 2015 Jul;9(1):095058.
- [3] Zhang, Y., Huston, D. and Xia, T., 2016, April. Underground object characterization based on neural networks for ground penetrating radar data. In Nondestructive characterization and monitoring of advanced materials, aerospace, and civil infrastructure 2016 (Vol. 9804, p. 980403). International Society for Optics and Photonics.
- [4] Zhang Y, Wang G, Xia T. Compressive orthogonal frequency division multiplexing waveform based ground
- [5] Y. Wang, "Bandwidth synthesis for stepped chirp signal: A multichannel sampling prospective," IET International Radar Conference 2013.
- [6] R. T. Lord and M. R. Inggs, "High range resolution radar using narrowband linear chirps offset in frequency," Proceedings of the 1997 South African Symposium on Communications and Signal Processing.
- [7] Soumekh, M., "Synthetic aperture radar signal processing with MATLAB algorithms", Wiley-Interscience (1999)
- [8] Utsi, Erica Carrick. Ground Penetrating Radar: Theory and Practice. Butterworth-Heinemann, an Imprint of Elsevier 2017.
- [9] Dang Hongxing, "Stepped frequency chirp signal SAR imaging," Asian and Pacific Conference on Synthetic Aperture Radar, 2007
- [10] W. Zhai and Y. Zhang, "A stepped frequency chirp scaling algorithm for high resolution SAR imaging," International Asia-Pacific Conference on Synthetic Aperture Radar (APSAR) 2011.
- [11] S. Prager, T. Thrivikraman, M. Haynes, J. Stang, D. Hawkins and M. Moghaddam, "Ultra-wideband synthesis for high-range resolution software defined radar," 2018 IEEE Radar Conference (RadarConf18).
- [12] S. C. Carey and W. R. Scott, "Software defined radio for stepped-frequency, ground-penetrating radar," 2017 IEEE International Geoscience and Remote Sensing Symposium (IGARSS).
- [13]S. Sharma, P. Jena, R. Kuloor, "Ambiguity Function Analysis of SFCW and Comparison of Impulse GPR and SFCW GPR", 9th International Radar Symposium, 2013.
- [14] Yuan Haojuan, Gao Meiguo and Liu Guoman, "Coherent spectrum synthesis of frequency-stepped chirp signal," IET International Radar Conference 2009.
- [15] X. Shibo, G. Jialong and W. Bocai, "Research on high resolution SAR based on frequency-stepped chirps," Asian-Pacific Conference on Synthetic Aperture Radar 2009.
- [16] H. J. Martínez, S. Alvarez and M. A. Yarlequé, "Assessing the performance of three type of UWB antennas for FMCW GPR imaging," 2018 International Conference on Electromagnetics in Advanced Applications (ICEAA).
- [17] Z. Zhao, M. Yao, X. Deng, K. Yuan, H. Li and Z. Wang, "A Novel Ionospheric Sounding Radar Based on USRP," in IEEE Geoscience and Remote Sensing Letters, vol. 14, no. 10, pp. 1800-1804, Oct. 2017.